

## **Modulation of Neuronal Cell Affinity of Composite Scaffolds Based on Polyhydroxyalkanoates and Bioactive Glasses**

Lorena R. Lizarraga-Valderrama<sup>1,2\*</sup>, Rinat Nigmatullin<sup>1,3\*</sup>, Bryan Ladino<sup>1</sup>, Caroline S. Taylor<sup>4</sup>, Aldo R. Boccaccini<sup>5</sup>, Jonathan C. Knowles<sup>6,7,8,9</sup>, Frederik Claeysens<sup>4</sup>, John W. Haycock<sup>4</sup> and Ipsita Roy<sup>1\*\*</sup>

<sup>1</sup>Applied Biotechnology Research Group, School of Life Sciences, College of Liberal Arts and Sciences, University of Westminster, London, UK.

<sup>2\*</sup>Research and Innovation Department, University of Plymouth, Plymouth, UK

<sup>3\*</sup>Bristol Composites Institute (ACCIS), University of Bristol, Bristol, UK

<sup>4</sup>Department of Materials Science and Engineering, University of Sheffield, Sheffield, UK.

<sup>5</sup>Department of Materials Science and Engineering University of Erlangen-Nuremberg, Erlangen, Germany.

<sup>6</sup>Division of Biomaterials and Tissue Engineering, UCL Eastman Dental Institute, London, WC1X 8LD, UK

<sup>7</sup>Department of Nanobiomedical Science and BK21 Plus NBM, Global Research Center for Regenerative Medicine, Dankook University, Cheonan, Republic of Korea, 518-10 Anseo-dong, Dongnam-gu, Cheonan, Chungcheongnam-do, South Korea

<sup>8</sup>The Discoveries Centre for Regenerative and Precision Medicine, UCL Campus, London, UK

<sup>9</sup>UCL Eastman-Korea Dental Medicine Innovation Centre, Dankook University, Cheonan 31114, Republic of Korea

\*Current address

\*\*Corresponding Author

## **Keywords**

nerve regeneration, nerve tissue engineering, bioactive glasses, polyhydroxyalkanoates, composite scaffolds

## **Abstract**

Biocompatibility and neuron regenerating properties of various bioactive glass (BG)/Polyhydroxyalkanoate (PHA) blend composites were assessed in order to study their suitability for peripheral nerve tissue applications, specifically as inner structure for nerve guidance conduits (NGCs). BG/PHA blend composites were fabricated using Bioactive glass® 45S5 (BG1) and BG 1393 (BG2) with the 25:75 P(3HO)/P(3HB) blend. Various concentrations of each BG (0.5, 1.0 and 2.5 % w/v) were used to determine the effect of BG on neuronal growth and differentiation, in single culture using neuronal cells and in a co-culture system along with SCs (SCs). NG108-15 cells exhibited good growth and differentiation on all the PHA blend composites showing that both BGs have good biocompatibility at 2.5, 1.0 and 0.5 % w/v within the PHA blend. The Young's modulus values displayed by all the PHA blend/BG composites ranged from 385.6 MPa to 1792.6 MPa, which are able to provide the required support and protective effect for the regeneration of peripheral nerves. More specifically, the tensile strength obtained in the PHA blend/BG1 (1% w/v) ( $10.0 \pm 0.6$  MPa) was found to be similar to that of rabbit peroneal nerve. This blend also exhibited the best biological performance in supporting growth and neuronal differentiation among all the substrates. The neurite extension on this composite was found to be remarkable with the neurites forming a complex connection network.

## **1. Introduction**

After injury, peripheral nerves are able to regenerate spontaneously as a result of the action of SCs (SCs) that promote a favourable environment for axonal growth. However, the regeneration and recovery of nerve function depends on the injury gap length and the type of lesion. Suturing of the two stumps (i.e., end-to-end suture) is a suitable and common method to bridge small gaps (less

than 2 mm). For larger gaps, nerve regeneration is severely impeded and repair of nerve tissue requires nerve grafting with an autologous nerve graft being accepted as the “gold standard” procedure.<sup>[1]</sup> However, common complications of autografting such as additional surgery, loss of nerve function, donor site morbidity and scar tissue formation limit the success of patient recovery.

Bioartificial tubular devices, widely known as nerve guidance conduits (NGCs) are a promising alternative to autografting. Neural tissue regeneration based on NGCs prevents additional surgical intervention required to harvest autologous nerves and thereby less surgical trauma is inflicted. Moreover, fibrous scar tissue infiltration is reduced whereas accumulation of soluble factors is maximized. Additionally, the use of NGCs avoids mismatched fascicles between the injured nerve and the autograft.<sup>[1]</sup> In addition to biocompatibility, a bioresorbable NGC has to be a mechanically robust device which combines good flexibility with compressive resistance, preventing compression of the growing nerve tissue or collapse of the tubular structure. There are several commercial NGCs made from natural and synthetic materials, such as poly(L-lactide-co-caprolactone) (PLCL), poly(glycolic acid) PGA, poly(vinyl alcohol) PVA, collagen type I and extracellular matrix (ECM) (Sarker *et al.*, 2018). The regeneration outcomes achieved with the current NGCs are comparable with the autologous nerve graft only for short gaps (less than 10 mm). For longer nerve defects, i.e. critical gaps, autografting performs better when compared with NGCs.

Hence, the main focus of further progress in NGCs is in the development of intraluminal architecture. Modifications in the lumen of NGCs have shown to enhance nerve regeneration *in vitro* and *in vivo*.<sup>[1]</sup> A range of different types of internal structures serving as physical cues have been explored including grooves, random and aligned fibres to guide neuronal growth, reducing neurite misdirection.<sup>[1,2]</sup> Both synthetic and natural polymers have been used for the manufacturing of such internal structures. However, with recent advances in applications of inorganic bioactive glasses (BGs) in soft tissue engineering,<sup>[2]</sup> BGs have recently been studied in nerve tissue regeneration. Despite the intrinsic brittleness of BGs, interest in their application for nerve regeneration is driven by the proven biological activity of BGs due to the leaching of bioactive ions. In contrast, polymers

provide a good support for cell growth, but they do not exhibit such an inherent release of factors with biological activity. Hence, bioactive glasses not only can enhance cell adhesion through the formation of a hydroxyapatite layer but also release ions that can trigger the cell signalling process, favouring tissue regeneration. [2]

Various types of BGs have been shown to have regenerative P(properties in a neuronal context. For example, Bioactive glass® 45S5 fibres are not only compatible with rat SCs and fibroblasts *in vitro*, but also demonstrate the promotion of axonal regeneration *in vivo*. [3] Phosphate glass fibres are biocompatible with the Neonatal Olfactory Bulb Ensheathing Cell Line (NOBEC) [1, 4] and Dorsal Root Ganglion (DRG) neurons. [4,5] Additionally, such fibres provide a directional cue for growing axons. [1,4] Moreover, bioactive borate glass scaffolds have not only shown biocompatibility with embryonic chick DRG but have also been shown to support neurite extension. [6] Mohammadkhah [7] fabricated composites using different BG compositions consisting of 50 wt% PCL combined with 50 wt% 13–93 B3 borate glass; 50 wt% 45S5 silicate glass and with a blend of 25 wt% 13–93 B3 and 25 wt% 45S5 silicate glass. The resulting composites were found to be compatible with DRG neurons isolated from embryonic chicks and had a positive effect on neurite outgrowth. [7] In order to overcome BG brittleness, both BG fibres [8] and BG particles [9] have been embedded into polymeric matrices.

Herein we have designed bioresorbable hybrid composites by combining a blend of bioresorbable polyhydroxyalkanoates (PHAs) with particulate BGs. BG/PHA blend composites were fabricated using Bioactive glass® 45S5 (BG1) and BG 1393 (BG2) with the 25:75 P(3HO)/P(3HB) blend. We extend our previously reported work [10] in the development of flexible PHA blends, which were highly biocompatible with neuronal cells and thereby provided a good support for growth of nerve tissue. Here we demonstrate that adding BGs as fillers to a 25:75 poly-3-hydroxyalkanoate/poly-3-hydroxybutyrate (P(3HO)/P(3HB) (PHA blend) has a further positive effect on the growth and differentiation of RN22 SCs and NG108-15 neuronalr cells. This effect depends on the BG content, confirming the biological activity of BGs incorporated in the

bioresorbable polymer matrices. Quite counter-intuitively, introduction of BGs decreased the stiffness of the PHA blends. This combination of suitable mechanical properties and enhanced ability to support growth and differentiation of neuronal cells confirmed the possible application of these highly bioactive composite scaffolds as internal guidance structures within the lumen of bioresorbable NGCs, to be used for critical gap repair.

## 2. Experimental Sesion

*Production and extraction of poly(3-hydroxyalkanoate) and poly(3-hydroxybutyrate):* Production, extraction, purification of both PHAs, P(3HO) and P(3HB), and the determination of lipopolysaccharides was carried out as described by Rai *et al.*, 2011. <sup>[11]</sup> Briefly, P(3HO) and P(3HB) were produced through bacterial fermentation using *Pseudomonas mendocina* and *Bacillus cereus* SPV followed by soxhlet extraction.

*Composite film preparation:* This study focuses on the evaluation of cellular response towards PHA-based composites which were conducted on planar surfaces. The chemical composition of BG1 and BG2 are shown in Table 1. Films of PHA blend along with BG1 and BG2 were prepared using the solvent casting method <sup>[10]</sup>. The PHAs were dissolved in chloroform (Sigma-Aldrich, Gillingham, UK) in order to obtain a total polymer concentration of 5 wt/vol % of the 25:75 P(3HO)/P(3HB) blend. After polymer dissolution, the required amounts of each bioactive glass were introduced into the polymer solution to obtain formulations containing 0.5, 1.0, 2.5 wt% of BG with respect to the PHAs. BGs were dispersed by sonication using a probe sonicator. The polymer solutions containing dispersed BGs were cast in 6-cm glass petri dishes. The films were air dried and produced in triplicate in order to obtain a total of twenty-one films including the control 25:75 P(3HO)/P(3HB) blend. Additionally, films of polycaprolactone (PCL), an established biocompatible and bioresorbable polymer, were used as a control polymeric material. PCL was provided by Vornia Biomaterials Ltd. (Dublin, Ireland). The PCL contained a methyl ether polyethylene glycol block which was used as an initiator in the ring opening polymerisation of caprolactone. This block made PCL relatively more hydrophilic. PCL films were prepared as described above for composite films using 5 wt % PCL solution in chloroform. All polymer films were aged for 5 weeks at room temperature. During this period crystallization of the polymers were expected to be completed for all samples (Lizarraga-Valderrama *et al.*, 2015).

*Scanning electron microscopy of PHAs/bioactive glass composites:* Surface topography of the films and the PHA/BG composites was analyzed using a FEI XL30 Field Emission Gun Scanning Electron Microscope (FEI, Netherlands). All the samples were previously sputter-coated with a 20 nm film of palladium using a Polaron E5000 sputter coater. The operating pressure of the sputter coating was  $5 \times 10^{-5}$  bar with a deposition current of 20 mA for a duration of 90 s. The images were then recorded and the diameters of pores were measured at different magnifications at 5kV using the FEI software.

*Profilometric surface analysis:* The surface roughness of the films was analyzed using a Sony Proscan 1000 Laser Profilometer (Sony, Japan) with a measuring range of 400  $\mu\text{m}$ , a resolution of 0.02  $\mu\text{m}$  and a maximum output of 10 mW. Scans of 0.5  $\text{mm}^2$  were obtained from each sample. Nine random coordinates were selected from each specimen in order to measure the Root Mean Square (RMS) roughness ( $R_q$ ) defined as the root mean square average of the profile height deviations from the mean line. The formula defining  $R_q$  is as follows:

$$\text{i) } R_q = \sqrt{\frac{1}{n} \sum_{i=1}^n y_i^2}$$

where  $n$  is the number of intersections of the profile at the mean line (intersections); and  $\gamma$ , profile slope at mean line ( $^\circ$ ) (Gadelmawla., *et al* 2002)

*Surface wettability of the films:* The wettability of the films was measured by using a KSV Cam 200 goniometer (KSV, Finland). About 200  $\mu\text{L}$  of deionized water was dropped onto the surface of the films using a gas-tight micro-syringe. As soon as the water droplet made contact with the sample, a total of 10 images were captured with a frame interval of one second. The analysis of the images was performed using the KSV Cam software. For each sample, three random points were analyzed to obtain a total of nine measurements for each type of film.

*Mechanical properties:* Tensile testing was carried out using a 5942 Instron Testing System (High Wycombe, UK) equipped with a 500N load cell at room temperature. The test was conducted using films of 5 mm width and length of 3.5-5 cm. The deformation rate was 5 mm/min. The average values for 5 specimens were calculated.

*Differential scanning calorimetry:* Thermal transitions for composites were characterized using DSC 214 Polyma (Netzsch, Germany), equipped with Intracooler IC70 cooling system. Scanning was conducted

between -70 °C and 200 °C at a heating rate of 10 °C/min under the flow of nitrogen at 60 mL/min. Enthalpy of fusion for P(3HB) was normalised to the weight fraction of P(3HB) in composites or a polymer blend.

*NG108-15 Neuronal and RN22 Schwann cell culture:* The NG108-15 cell line is a hybrid of mouse neuroblastoma and rat glioma whereas RN22 SCs are obtained from rats. These were grown in DMEM under a humidified atmosphere of 5 % CO<sub>2</sub> at 37°C. The Dulbecco's Modified Eagle Medium (DMEM) (Sigma-Aldrich, Gillingham, UK) was supplemented with 10 % (v/v) fetal calf serum (Sigma-Aldrich, Gillingham, UK), 1 % (w/v) glutamine (Sigma-Aldrich, Gillingham, UK), 1% (w/v) penicillin/streptomycin (Sigma-Aldrich, Gillingham, UK), and 0.5% (w/v) amphotericin B (Sigma-Aldrich, Gillingham, UK). Cells were only used in the experiments once they were 80 % - 90 % confluent. For the single culture of NG108-15, the cells were trypsinised and  $3 \times 10^4$  cells of NG108-15 were seeded directly onto the PHA film samples within the 12 well plates in 3 mL of DMEM (Sigma-Aldrich, Gillingham, UK). The cultures were maintained for 4 days, with half of the media being removed and replaced with fresh serum-free DMEM (Sigma-Aldrich, Gillingham, UK) on day 2 to trigger differentiation. The NG108-15 neuronal cells were used between passages 10-20 while RN22 cells between 15-25 passages. For co-culture with RN22 SCs,  $1.5 \times 10^4$  cells of each cell type were trypsinised and were seeded in the same well directly onto the PHA film samples and cultures were maintained for 4 days, with half of the media being removed and replaced with fresh serum-free DMEM (Sigma-Aldrich, Gillingham, UK) on day 2 to trigger differentiation.

*Live/dead measurement of NG108-15 neuronal cells:* After growing the cells for 4 days, the culture medium was removed and replaced with fresh serum-free DMEM (Sigma-Aldrich, Gillingham, UK) containing 0.0015% (w/v) propidium iodide (Invitrogen, 55B Bridge Cl, Dartford DA2 6PT, UK) and 0.001% (w/v) 0.4Syto-9 (Invitrogen, Dartford, UK) at 37°C/5% CO<sub>2</sub> for 15 min. After washing with phosphate-buffered saline (PBS) (x3), the cells were imaged by confocal microscopy. A helium-neon laser was used for the detection of propidium iodide ( $\lambda_{ex}$ = 536 nm/ $\lambda_{em}$ =617 nm) (Invitrogen, 55B Bridge Cl, Dartford DA2 6PT, UK) while an argon-ion laser was used for Syto 9 ( $\lambda_{ex}$ = 494 nm/ $\lambda_{em}$  = 515 nm). Three fields-of-view were imaged containing 20-500 cells per sample, so as to express the data as a percentage of live versus dead cells  $\pm$  Standard Error of the Mean (SEM). Quantification of live and dead cells was performed using Image J.

*Immunolabelling of NG108-15 neuronal cells and RN22 SCs:* To assess the differentiation of NG108-15 neuronal cells, cells were labelled for  $\beta$  III-tubulin (neurite marker). Samples containing cultures of NG108-15 neuronal cells were washed with PBS (x3) (Sigma–Aldrich, Gillingham, UK) and fixed with 4% (v/v) paraformaldehyde (Sigma–Aldrich, Gillingham, UK) for 20 min at room temperature. Cells were permeabilized with 0.1 % (v/v) Triton X-100 (Sigma–Aldrich, Gillingham, UK) for 20 mins, before being washed with PBS (Sigma–Aldrich, Gillingham, UK) (x3). Unreactive binding sites were blocked with 3% (w/v) bovine serum albumin (BSA) (Sigma–Aldrich, Gillingham, UK) for 30 mins, at room temperature, and cells were incubated overnight with a mouse anti  $\beta$  III-tubulin antibody (1:1000) (Sigma–Aldrich, Gillingham, UK) diluted in 1% BSA (Sigma–Aldrich, Gillingham, UK) at 4°C. In the case of co-cultures, polyclonal rabbit anti-S100 $\beta$  diluted in 1% BSA at 4 C was also added (Schwann cell marker for co-cultures) (1:250) (Dako, Denmark). Cells were then washed three times with PBS (Sigma–Aldrich, Gillingham, UK) before being incubated either with Texas Red-conjugated anti-mouse IgG antibody (1:100 dilution in 1% BSA) (Sigma–Aldrich, Gillingham, UK), and for co-cultures, also a FITC-conjugated secondary anti-rabbit IgG antibody (1:100 in 1% BSA) (Vector Labs, USA) for 90 mins at room temperature. After washing the cells once with PBS, 4', 6-diamidino-2-phenylindole dihydrochloride (DAPI) (1:500 dilution in PBS) was added to label nuclei. Cells were then incubated for 30 mins at room temperature before being washed again with PBS (x3). Cells were then imaged by using confocal microscopy. Nuclei were visualized by two photon excitation using a Ti:sapphire laser (716 nm) for DAPI ( $\lambda_{ex} = 358 \text{ nm}/\lambda_{em} = 461 \text{ nm}$ ) (Sigma–Aldrich, Gillingham, UK). For imaging the neuronal cell body and neurites of NG108-15 cells, a helium-neon laser (543nm) was used to detect Texas Red-conjugated anti-mouse IgG antibody (1:100 dilution in 1% BSA) ( $\lambda_{ex} = 589 \text{ nm}/\lambda_{em} = 615 \text{ nm}$ ) (Sigma–Aldrich, Gillingham, UK). For imaging RN22 Schwann cell cytoskeleton, an argon ion laser (488 nm) was used to detect FITC ( $\lambda_{ex} = 495 \text{ nm}/\lambda_{em} = 521 \text{ nm}$ ) (Sigma–Aldrich, Gillingham, UK). The differentiated cells were then counted using Image J and identified as neuronal cells expressing neurites.

*Statistical analysis:* A Shapiro - Wilk and Bartlett's test was previously performed to verify the normality and homogeneity of the data respectively. To analyse the difference between data, a one-way ANOVA test ( $p < 0.05$ ) was conducted followed by Turkey's – post test ( $p < 0.05$ ). Data was reported as mean  $\pm$  SEM.

### **3. Results and Discussion**



### 3.1. Structural and mechanical characterisation of composite scaffolds

The selection of a polymer matrix for the preparation of new composites suitable for nerve regeneration was based on our previous study of binary PHA blends combining the rigid and strong P(3HB), with the soft and elastomeric P(3HO).<sup>[10]</sup> In that study, the 25:75 P(3HO)/P(3HB) blend was identified as the most promising material for supporting the growth of neuronal cells. Therefore, a blend of this composition was used as a matrix for the preparation of BG composites and is referred as PHA blend throughout this paper. Two types of BGs, BG1 and BG2 were incorporated into the polymer matrix via processing of polymer solutions in chloroform. The chemical composition of both bioactive glasses is shown in Table 1. The BGs used in this study are different in chemical composition and also in particle size. The average particle size of BG1 was about 4  $\mu\text{m}$  in diameter and had a clearly narrower particle size distribution than BG2 (Supporting information, Figure S1). Particles of BG2 were between 3 to 15  $\mu\text{m}$  in diameter.

**Table 1.** Chemical composition of 455S Bioactive glass® and BG 1393

| Bioactive glass | Composition (wt %)  |
|-----------------|---|
| BG 45S5         | 45 SiO <sub>2</sub> , 24.5 CaO, 24.5 Na <sub>2</sub> O, 6 P <sub>2</sub> O <sub>5</sub>                         |
| BG 1393         | 53 SiO <sub>2</sub> , 20 CaO, 6 Na <sub>2</sub> O, 4 P <sub>2</sub> O <sub>5</sub> , 12 K <sub>2</sub> O, 5 MgO |

The PHA blend tended to form porous films with pores of an average size of  $1.6 \pm 0.2 \mu\text{m}$ , uniformly distributed across the film surface (Figure 1 M, N). Films of polycaprolactone (PCL) were also prepared using the same conditions, to act as another control material. The PCL control film exhibited significantly larger pores with an average diameter of  $36.1 \pm 3.5 \mu\text{m}$  (Figure 1 O, P). The incorporation of two different BGs to the PHA blend caused dissimilar changes in surface morphology; films of PHA blend/BG2 (Figure G-L) composites were notably less porous in comparison to composites filled with BG1 (Figure A-F). This was probably related to differences in the distribution of BG particles of different particle size distribution. It is well known that an increase in polydispersity of particles leads to a decrease in void volume when the particles are packed.<sup>[12]</sup> This is also valid for porous particle-polymer composites.<sup>[13]</sup> Wider size distribution of the BG2

particles allows denser packing of the BG2 particles in the polymer matrix resulting in relatively less porous composite films. Generally, addition of BGs led to larger pores compared to the pores on the PHA blend control. The most developed porosity was achieved for the PHA blend/BG1 (0.5 wt %) and PHA blend/BG1 (2.5 wt%) which showed intricate porous networks with an average pore size of  $5.4 \pm 0.7 \mu\text{m}$  and  $3.5 \pm 0.3 \mu\text{m}$ , respectively (Figure 1 A-B, E-F). Although no relationship was found between the amount of BG and the pore size, in the context of materials development for internal structures of NGCs it is important that BG additives allow maintenance or even improve the material porosity. Porosity is considered as a crucial structural feature of materials which provides an efficient cell migration, nutrient and catabolite exchange <sup>[14]</sup> required for nerve regeneration. It is worth noting that the pore size for the composites developed in this study (3–10  $\mu\text{m}$ ) are within the 5–30  $\mu\text{m}$  range recommended for NGCs, hence a lumen coat using these PHA-composites will fulfill the adequate porosity. <sup>[14]</sup>

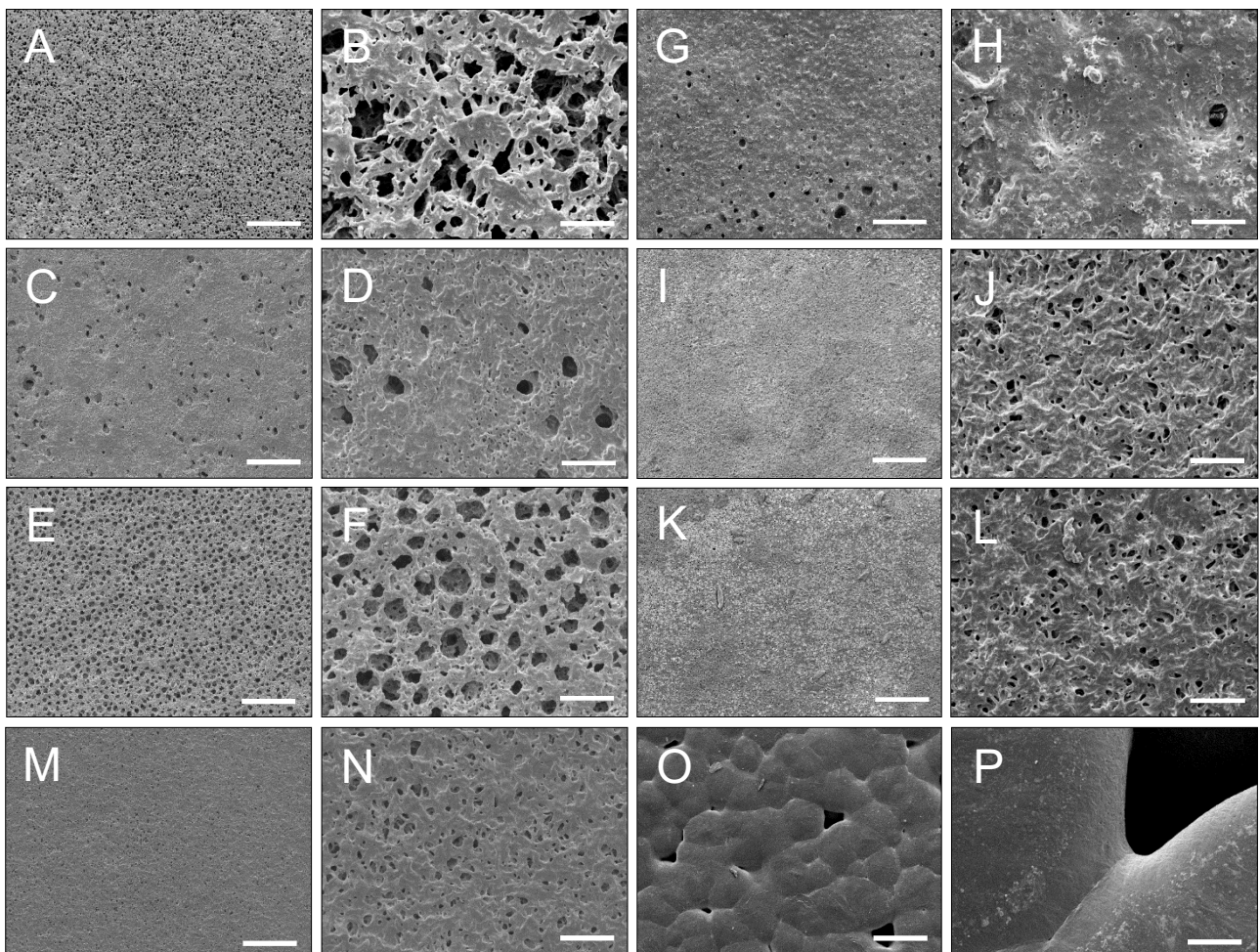


**Figure 1.** Scanning electron microscopy of PHA blend/BG composites and controls. (A, B) PHA blend/BG1 (0.5 wt %). (C, D) PHA blend/BG1 (1.0 wt %). (E, F) PHA blend/BG1 (2.5 wt %). (G, H) PHA blend/BG2 (0.5 wt %). (I, J) PHA blend/BG2 (1.0 wt %), (K, L) PHA blend/BG2 (2.5 wt %). (M, N) PHA blend. (O, P) PCL. Scale bar: 100  $\mu\text{m}$  – first and third column; 10  $\mu\text{m}$  – second and fourth column.

Compared to the series of PHA blend/BG1 composites, the surface morphology of PHA blend/BG2 composites were less regular with the occurrence of protrusions (Figure 1 G-L). The protrusions were most likely formed due to the presence of much larger particles in BG2. As a result, the roughness, determined as the root mean square roughness ( $R_q$ ) by laser profilometry, was systematically higher for the PHA blend/BG2 composites (Figure 2). The incorporation of BG2 resulted in rougher surfaces for composites containing 0.5 wt % and 2.5 wt % of BG2 ( $2.6 \pm 0.1 \mu\text{m}$  and  $2.3 \pm 0.01 \mu\text{m}$ , respectively) compared with the PHA blend control ( $1.2 \pm 0.1 \mu\text{m}$ ), while roughness of the PHA blend/BG2 (1.0 wt %) was not significantly different to that of the PHA blend control. At the same time, incorporating BG1 led to decreased  $R_q$  values in comparison with the control PHA blend film (Figure 2). Interestingly, the roughness of the PHA blend/BG1 (1.0 wt %) and PHA blend/BG2 (0.5 wt %), the least porous samples in each composite series, was higher compared with the more porous samples of the corresponding composite series. The two other control surfaces used in the study provided examples of smooth ( $0.3 \pm 0.0 \mu\text{m}$  for the glass slide) and highly rough ( $7.2 \pm 0.1 \mu\text{m}$  for PCL film) surfaces.

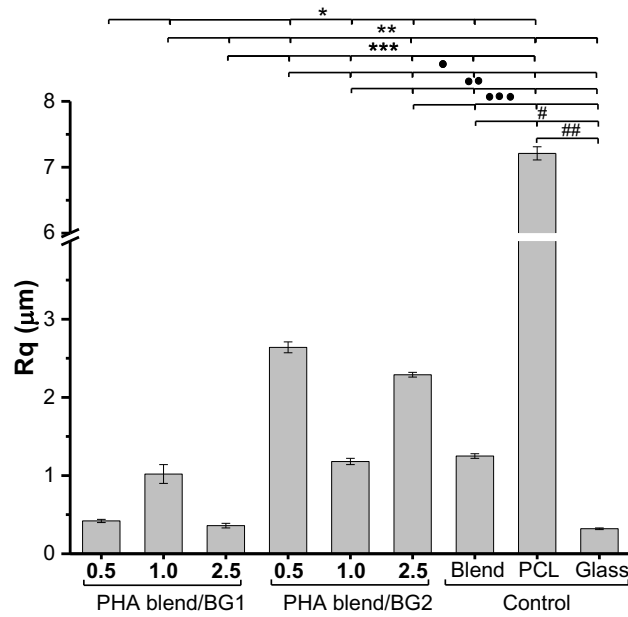


**Figure 2.** Root mean square roughness (Rq) of the PHA blend/bioactive glass composites and controls. The roughness presented by the PHA blend/BG1 composites was lower compared with PHA blend/BG2 composites. The highest roughness value was displayed by the PCL substrate.

As seen in Figure 2, the roughness of the PHA blend/BG1 (0.5 wt %) was not statistically different to PHA blend/BG1 (2.5 wt %) and glass ( $0.4 \pm 0.0 \mu\text{m}$ ,  $0.4 \pm 0.0 \mu\text{m}$ ,  $0.3 \pm 0.0 \mu\text{m}$  respectively,  $*p < 0.05$ ). The lowest roughness was displayed by the glass slide control compared to all the substrates. The roughness of PHA blend/BG1 (1.0 wt %) was not significantly different to that of PHA blend/BG2 (1.0 % w/v) and the PHA blend ( $1.0 \pm 0.1$ ,  $1.2 \pm 0.1 \mu\text{m}$ ,  $1.3 \pm 0.0 \mu\text{m}$  respectively,  $**p > 0.05$ ) and significantly lower than those measured for the PHA blend/BG2 (0.5 wt %) and PHA blend/BG2 (2.5 wt %) ( $2.6 \pm 0.1 \mu\text{m}$ ,  $2.3 \pm 0.0 \mu\text{m}$ ,  $**p < 0.05$ ). The PHA blend/bioactive glass composites that displayed the highest roughness were PHA blend/BG2 (0.5 wt %) ( $2.6 \pm 0.1$ ,  $p < 0.05$ ) and PHA blend/BG2 (2.5 wt %) ( $2.3 \pm 0.0$ ,  $p < 0.05$ ). The highest roughness among all the substrates was presented by the PCL control ( $7.2 \pm 0.1 \mu\text{m}$ ,  $p < 0.05$ ).

Surface hydrophilicity is a simple determinant of cellular response towards biomaterials. Previous studies have shown that cell attachment increases when hydrophilicity increases. These findings have been observed for different cell types such as osteoblasts, <sup>[15,16]</sup> fibroblasts, <sup>[17,18]</sup> Madin-Darby Canine Kidney (MDCK) cells, <sup>[19]</sup> mouse osteoblast-like cell line MC3T3-E, <sup>[18]</sup> 7F2

mouse osteoblasts <sup>[20]</sup> and neurites.<sup>[21,22]</sup> PHA/BG composites combine a hydrophobic polymer with hydrophilic fillers, hence, the surface hydrophilic/hydrophobic balance was expected to vary depending on the BG content. The water contact angles were measured for all substrates as a widely used parametre of surface hydrophilicity/wettability (Table 2).

**Table 2.** Water contact angles of PHA blend/BG composites and controls.

| Substrates              | Water contact angle (°) |
|-------------------------|-------------------------|
| PHA blend/BG1 (0.5wt %) | 95.7 ± 0.6              |
| PHA blend/BG1 (1wt %)   | 65.7 ± 1.2              |
| PHA blend/BG1 (2.5wt %) | 65.3 ± 1.4              |
| PHA blend/BG2 (0.5wt %) | 93.5 ± 0.8              |
| PHA blend/BG2 (1wt %)   | 78.8 ± 0.7              |
| PHA blend/BG2 (2.5wt %) | 67.0 ± 0.7              |
| PHA blend               | 77.4 ± 0.8              |
| PCL                     | 81.9 ± 1.3              |
| Glass                   | 23.2 ± 0.5              |

In both series of composites there was a significant decrease in surface wettability for composites with the lowest BG content; contact angles of  $95.7^\circ \pm 0.6^\circ$  and  $93.5^\circ \pm 0.8^\circ$  for PHA blend/BG1 (0.5 wt %) and PHA blend/BG2 (0.5 wt %), respectively, compared with  $77.4^\circ \pm 0.8^\circ$  for the control PHA blend. Such an increase reflects the contribution of surface topography to the change in surface wettability. Although the roughness for the PHA blend/BG1 (0.5 wt %) did not significantly change compared with the PHA blend, the technique used in this study evaluates roughness on a micrometer scale. Probably topographical features of nano- and submicron sizes in the composite film resulted in an increase in the contact angle for these composites. BG particles were completely covered with the polymer matrix in composites with 0.5 wt % BG content, when particle/polymer ratio was low. In this case, hydrophilicity of the BG did not contribute to the wettability. However, with the increase in BG content more BG particles were exposed on the composite surface, increasing the surface hydrophilicity and the contact angle decreased with respect to PHA blend for composites containing 1.0 wt% and 2.5 wt% BG. Composites with filler content of 1.0 wt% and 2.5 wt% showed lower contact angle values than the PHA blend except for PHA

blend/BG2 (1.0 wt%). Slightly lower values of contact angles for the composites filled with BG1 is likely due to their surfaces being smoother as compared with composites containing BG2.

The materials were further characterised by differential scanning calorimetry (DSC) to evaluate the influence of inorganic fillers in crystallisation and the state of the amorphous phase of semi-crystalline PHAs. DSC thermograms (Supporting information, Figure S2) show that composites and the control PHA blend did not exhibit melting of the P(3HO) component. Thus P(3HO) was not crystallised as a single phase in the P(3HB) matrix. Although the melting temperature of P(3HB) was not affected by the presence of BG, the degree of crystallinity of P(3HB) significantly decreased in the composites with BG1 (Table 3) compared with the control PHA blend and crystallinity gradually decreased with the increase of filler content. On the other hand, it appears that P(3HB) crystallinity was not influenced by BG2: 65.8, 64.0, 67.4% for composites containing 0.5, 1.0 and 2.5wt % of BG2, respectively, compared to 65.6% for the PHA blend. In the composites, crystallisation of P(3HB) occurs in a confined space between the BG particles. Less polydisperse particles of BG1 perhaps formed a more regularly packed environment than BG2. Additionally, as was discussed above, composites with BG1 were more porous than the PHA blend / BG2 composites. These two factors could drive the P(3HB) crystallisation to occur in a more confined space for the PHA blend / BG1 composites resulting in the suppression of P(3HB) crystal growth. The higher the BG content the more crowded the system would be, leading to a lower degree of P(3HB) crystallisation (Table 3). However, in the case of PHA blend / BG2 composites, higher degree of BG packing might lead to the formation of BG-rich and BG-depleted regions. Hence, in this case, P(3HB) crystallisation was similar to the crystallisation in the PHA blend.

**Table 3.** Differential scanning calorimetry of PHA blend/BG composites.

| Substrates               | T <sub>g</sub> (°C) | T <sub>m</sub> (°C) | Specific enthalpy of melting (kJ/g) |                      | X <sub>c</sub> , %* |
|--------------------------|---------------------|---------------------|-------------------------------------|----------------------|---------------------|
|                          |                     |                     | Observed                            | Normalised to P(3HB) |                     |
| PHA blend/BG1 (0.5 wt %) | n/d                 | 177.6               | 59.2                                | 79.5                 | 54.4                |
| PHA blend/BG1 (1 wt %)   | n/d                 | 175.1               | 42.0                                | 56.8                 | 38.9                |
| PHA blend/BG1 (2.5 wt %) | n/d                 | 173.0               | 36.8                                | 50.8                 | 34.5                |
| PHA blend/BG2 (0.5 wt %) | n/d                 | 174.6               | 71.2                                | 95.5                 | 65.8                |
| PHA blend/BG2 (1 wt %)   | n/d                 | 174.3               | 69.2                                | 93.5                 | 64.0                |
| PHA blend/BG2 (2.5 wt %) | n/d                 | 174.4               | 71.3                                | 98.4                 | 67.4                |
| PHA blend                | n/d                 | 174.6               | 71.8                                | 95.7                 | 65.6                |

\* the crystallinity degree of P(3HB) was calculated using the formula  $X_C = \frac{\Delta H_{norm}}{\Delta H_0} \times 100$  and  $\Delta H_0 = 146 \text{ J/g}$ .<sup>[23]</sup>

Interestingly, for all the composites and the PHA blend the glass transition event was not detected (Table 3) in the temperature range where the glass transition of P(3HB), the dominant component of the blend (close to 3°C), would be typically observed. The absence of glass transition indicated that the P(3HB) in the amorphous phase was in a rigid state, which is a vitrified state of the amorphous material.<sup>[24]</sup> Since the fractions of polymers in an amorphous state (Table 3) were significantly higher in the PHA blend/BG1 composites than in the PHA blend/BG2 composites, this is a further confirmation of our assumption of a more confined and regular space formed between less polydisperse BG1 particles and P(3HB) crystallites. The interface area is expected to be larger in such structures. As a result, despite the increased fraction, all amorphous polymers in PHA blend / BG1 composites distributed into the interfaces, which limited their mobility and transformed them into a rigid state.

Such differences in the rigidity of the amorphous phase and crystallisation for the two types of composites defined the mechanical properties of the materials. As can be seen from Table 4, PHA blend/BG1 composites were significantly softer than composites filled with BG2 and the control PHA blend. The Young's modulus decreased by 2-5 times for the PHA blend/BG1 composites, which was a result of the lower degree of crystallinity of P(3HB) in the polymer matrix. It is worth noting that

calculations of Young's modulus and ultimate strength do not take into consideration the porosity of the materials. However, the differences in the porosities of the materials were not so large and could not be the reason for such a decrease in the stiffness of composites filled with BG1. Counterintuitively, despite the presence of rigid BG1 in the polymer matrix, the flexibility of the PHA blend/BG1 composites significantly increased when compared with the PHA control; more than 15 times increase in elongation at break was observed for the PHA blend/BG1 composite (0.5 wt%) as compared to the PHA blend (Table 4). However, as expected, a further increase in BG content resulted in a decrease in the elongation at break within each series of the composites. All PHA blend/BG1 composites showed higher elongation at break values than the PHA blend/BG2 composites with equivalent BG content and also the control PHA blend.

**Table 4.** Mechanical properties of the PHA blend/Bioactive Glass composites

| Substrates               | Young's Modulus (MPa) | Ultimate tensile strength (MPa) | Elongation at break, % |
|--------------------------|-----------------------|---------------------------------|------------------------|
| PHA blend/BG1 (0.5 wt %) | 400.0 ± 6.0           | 5.8 ± 0.1                       | 36.0 ± 6.4             |
| PHA blend/BG1 (1 wt %)   | 850.0 ± 70.0          | 10.0 ± 0.6                      | 2.5 ± 0.3              |
| PHA blend/BG1 (2.5 wt %) | 390.0 ± 26.0          | 5.1 ± 0.7                       | 2.3 ± 0.5              |
| PHA blend/BG2 (0.5 wt %) | 1300.0 ± 100.0        | 16.1 ± 0.7                      | 3.6 ± 1.2              |
| PHA blend/BG2 (1 wt %)   | 1060.0 ± 50.0         | 13.0 ± 1.4                      | 1.7 ± 0.1              |
| PHA blend/BG2 (2.5 wt %) | 1730.0 ± 76.0         | 19.6 ± 0.8                      | 1.7 ± 0.2              |
| PHA blend                | 1800.0 ± 200.0        | 19.7 ± 0.3                      | 1.6 ± 0.1              |
| PCL                      | 390.0 ± 26.0          | 12.6 ± 0.3                      | 120.0 ± 41.0           |

Similar to the stiffness, the ultimate tensile strength was lower for PHA blend / BG1 composites. However, there was no correlation between the BG content and composite stiffness and strength, which are commonly described for composites by the rule of mixtures. The main reasons for this anomalous behaviour are variable porosity of the materials, variation in the crystallinity degree and perhaps poor compatibility between the polymer matrix and fillers. As a result of the interplay of these factors, the stiffest and strongest composites were achieved for composites containing 1.0 wt% of BG1 (Young's modulus and ultimate strength 850.0 ± 70.0 and 10.0 ± 0.6 MPa, respectively) and 2.5 wt% of BG2 (Young's modulus and ultimate strength 1730.0 ± 76.4 and 19.6 ± 0.8MPa, respectively). The tensile strength obtained in the PHA blend/BG1 (1% w/v) (10.0 ±



0.6 MPa) was found to be similar to that of rabbit peroneal nerve determined in another study ( $11.7 \pm 0.7$  MPa). [25]

### 3.2. Cellular response to the PHA-based composites

Primary evaluation of the biocompatibility of the PHA blend / BG composites was conducted using live/dead cell viability assay for NG108-15 neuronal cells. As shown in Figure 3, NG108-15 neuronal cells attached well and grew on the surface of all PHA-based materials. Cell growth was significantly lower on the glass control. A significant difference was found between the percentage of live cells on the control PHA blend ( $94.9 \pm 0.9$  %) and PCL film ( $92.4 \pm 1.6$  %) ( $\#P < 0.05$ ) implying superior neuronal growth for PHA-based materials compared with the widely used biodegradable PCL (Figure 3J). The percentage of live cells determined for all the composites was similar and found to be in the range of  $99.4 \pm 0.1$  % to  $92.4 \pm 1.6$  % (Figure 3J). These values were not significantly different as compared to the control PHA blend. Although the comparison of percentage of live cells did not display significant differences, the statistical analysis of the number of neuronal cells grown on the substrates revealed some differences in cell attachment for the composites. In Figure 3K the number of neuronal cells grown on different substrates was compared. The composite PHA blend/BG1 (1.0 wt %) supported the highest number of cells ( $760 \pm 60$  cells) among all the composites, which was significantly different when compared to the rest of the substrates ( $**P < 0.05$ ). On the other hand, the PHA blend/BG1 (0.5wt %) supported the lowest number of neuronal cells ( $215 \pm 30$  cells), presenting similar values when compared with the number of cells grown on the control PHA blend and PCL. Smaller variations in the number of viable cells were observed in the series of composites with the BG2 filler:  $400.0 \pm 110.0$ ;  $410.0 \pm 70.0$ ;  $250.0 \pm 45.0$  cells for PHA blend/BG2 (0.5 wt %), PHA blend/BG2 (1.0 wt %) and PHA blend/BG2 (2.5 wt %), respectively. In both series of composites decreased number of viable cells was found for the composites with 2.5 wt% BG content compared with the composites containing 1.0 wt% of BGs.

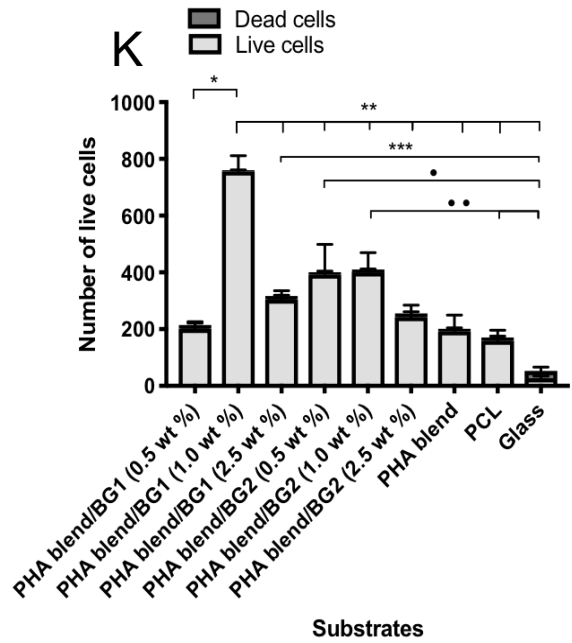
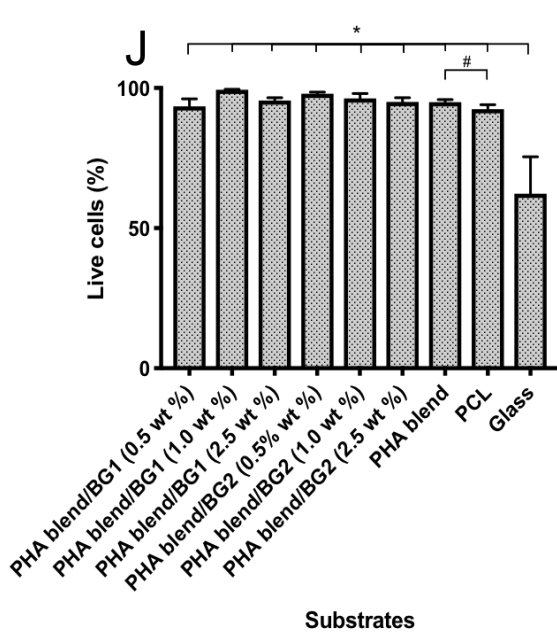
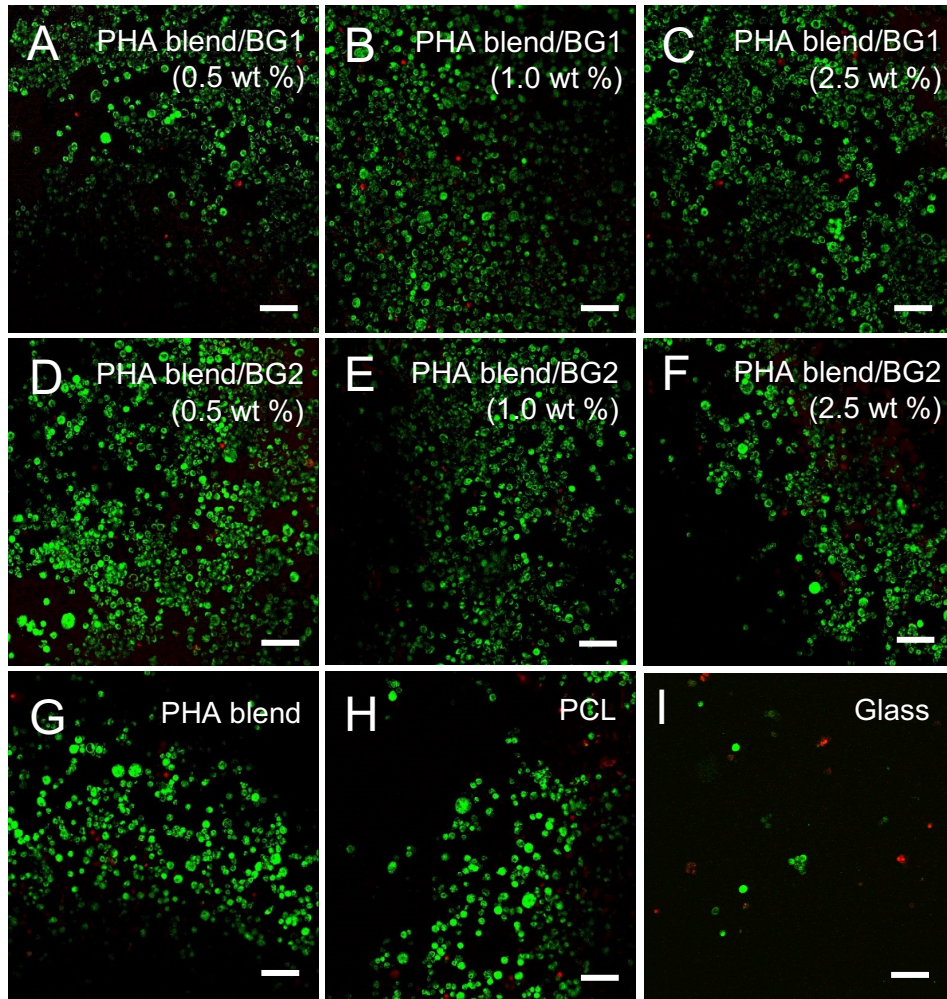


**Figure 3.** Confocal micrographs of NG108-15 neuronal cells labelled with propidium iodide (red) and Syto-9 (green) after four days in culture on PHA/Bioactive glass composites and the controls PHB blend, PCL and glass. A) PHA blend/BG1 (0.5 wt %), B) PHA blend/BG1 (1.0 wt %), C) PHA blend/BG1 (2.5 wt %), D) PHA blend/BG2 (0.5 wt %), E) PHA blend/BG1 (1.0 wt %), F) PHA blend/BG2 (2.5 wt %), G) PHB blend, H) PCL, I) and Glass. J) Live/dead analysis of neuronal cells on the P(3HO)/P(3HB) blends, PCL and glass (control).

As seen in Figure 3, the percentage of live neuronal cells on all the PHA blend/BG composites, PHA blend and PCL was higher in comparison to glass (control) (mean  $\pm$  SEM, n = 9 independent experiments \*P < 0.05). Percentage of live neuronal cells on the PHA blend was significantly different to the PCL control (mean  $\pm$  SEM, n = 9 independent experiments #P < 0.05. K) Number of live cells on PHA/bioactive glass composites, PHA blend, PCL and glass (control). The number of live cells grown on PHA blend/BG1 (1.0 wt %) was significantly different compared to the rest of substrates (760.0  $\pm$  60.0 cells). The number of neuronal cells displayed by PHA blend/BG1 (2.5 wt %) (317.0  $\pm$  30.0 cells) (\*\*P < 0.05) and PHA blend/BG2 (0.5 wt %) (400.0  $\pm$  110.0 cells) (\* P < 0.05) were found significantly different to the glass control (53.0  $\pm$  18.0 cells). Also, the number of cells grown on the PHA blend/BG2 (1.0 wt %) (410.0  $\pm$  70.0 cells) (\*\*P < 0.05) was significantly different to that grown on the controls, PCL (171.0  $\pm$  39.0) and glass (53.0  $\pm$  18.0 cells).

NG108-15 neuronal cells grown on the substrates were immunolabelled for anti- $\beta$  III-tubulin to study neuronal differentiation and neurite outgrowth. Neurite outgrowth assessment of NG108-15 neuronal cells was carried out according to the protocol of Daud [26]. Differentiation was confirmed in all the neuronal cells by the observed neurites sprouting in all the PHA blend/BG composites (Figure 4). However, more uniformly distributed and higher number of differentiated cells was found on the PHA blend/BG composites compared to the PCL and glass controls. It can be seen in Figure 4 that cells grown on PCL and glass were grouped in clusters with globular forms

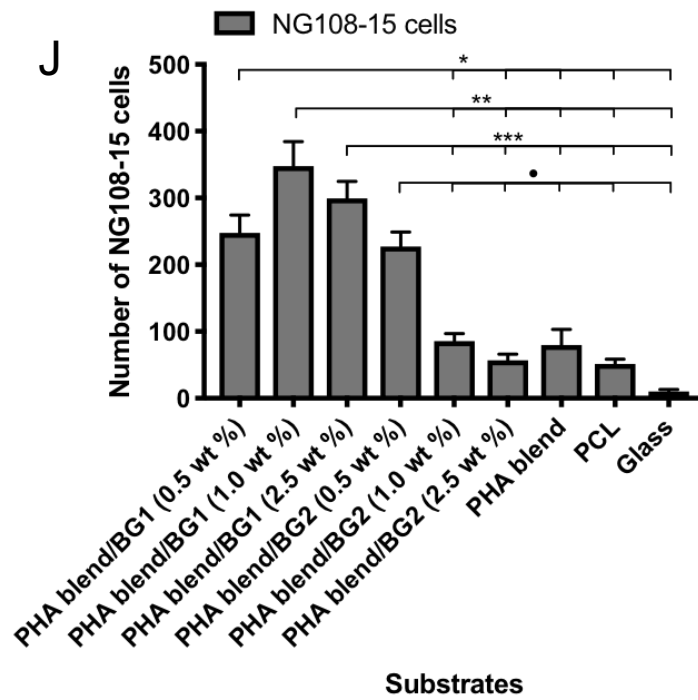
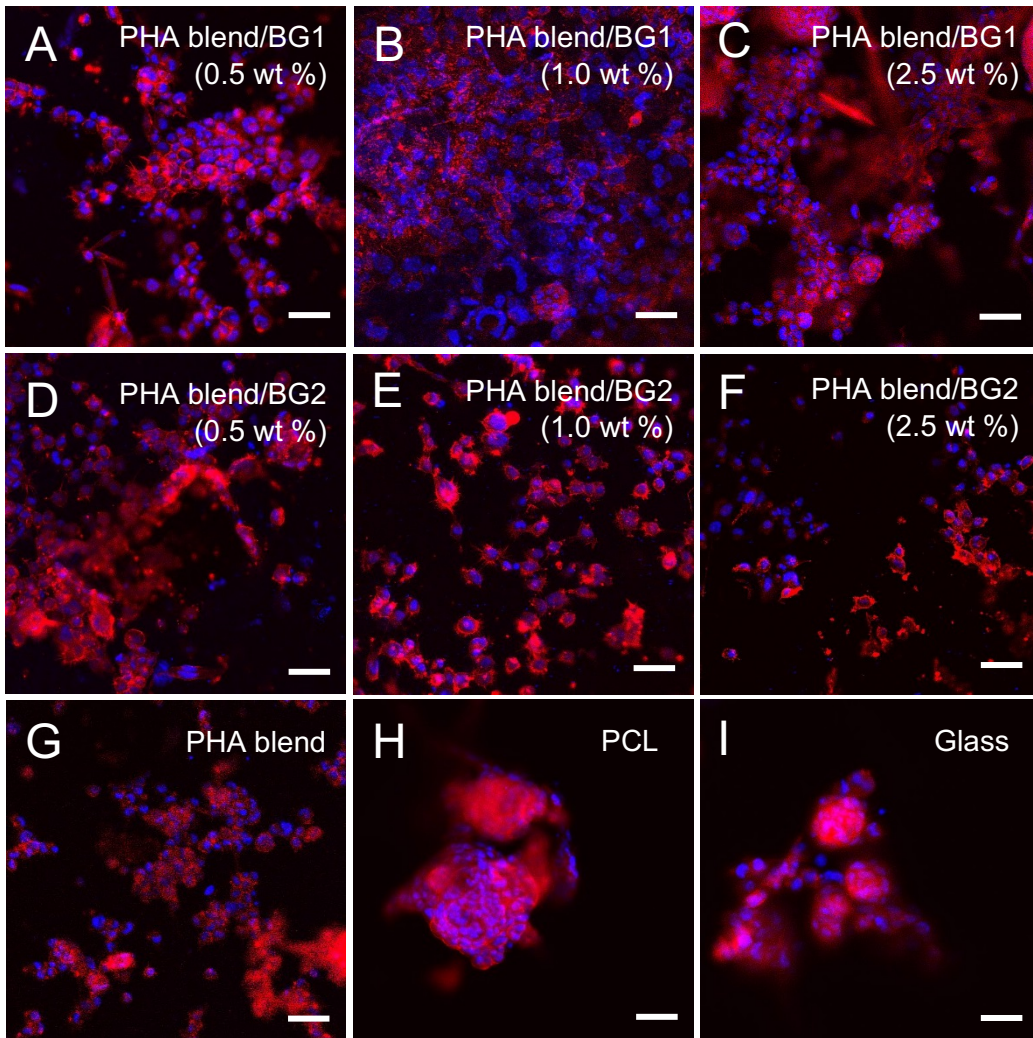


**Figure 4.** Micrographs of NG108-15 neuronal cells immunolabelled for  $\beta$ -III tubulin after 4 days culture on PHA blend composites. A) PHA blend/BG1 (0.5 wt %) composite, B) PHA blend/BG1 (1.0 wt %) composite, C) PHA blend/BG1 (2.5 wt %) composite, D) PHA blend/BG2 (0.5 wt %) composite, E) PHA blend/BG2 (1.0 wt %) composite, F) PHA blend/BG2 (2.5 wt %) composite, G) PHB blend, H) PCL, and I) Glass. J) Number of differentiated neuronal cells grown on substrates.

As seen in Figure 4, the PHA blend/BG1 (1.0 wt %) composite supported the highest number of differentiated neuronal cells ( $350.0 \pm 40$  cells) compared to the rest of substrates. The number of NG108-15 cells grown on the composites, PHA blend/BG1 (0.5 wt %) ( $230.0 \pm 20.0$  cells), PHA blend/BG1 (1.0 wt %) ( $350.0 \pm 40.0$  cells), PHA blend/BG1 (2.5 wt %) ( $300.0 \pm 25$  cells), PHA blend/BG2 (0.5 wt %) were significantly different to those found on PHA blend/BG2 (1.0% wt) ( $85.0 \pm 10.0$  cells), PHA blend/BG2 (2.5 wt %) ( $60.0 \pm 9.0$  cells) and the controls PHA blend film ( $80.0 \pm 23.0$ ), PCL film ( $50.0 \pm 7.0$  cells) and glass ( $10.0 \pm 3.0$  cells) (\*P < 0.05, \*\*P < 0.05, \*\*\*P < 0.05, • P < 0.05).

In line with the live/dead assay, the PHA blend/BG1 (1.0 wt %) composite supported the highest number of differentiated neuronal cells ( $350.0 \pm 40.0$  cells) in comparison to the rest of the substrates (Figure 4J). The total number of neuronal cells grown on the composites, PHA blend/BG1 (0.5 wt %) ( $230.0 \pm 20.0$  cells), PHA blend/BG1 (1 wt %) ( $350.0 \pm 40.0$  cells), PHA blend/BG1 (2.5 wt %) ( $300.0 \pm 25.0$  cells), and PHA blend/BG2 (0.5 wt %) ( $230.0 \pm 20.0$  cells), were significantly different to those found on the PHA blend/BG2 (1 wt %) ( $85.0 \pm 10.0$  cells), PHA blend/BG2 (2.5 wt %) ( $60.0 \pm 9.0$  cells) and the controls PHA blend film ( $80.0 \pm 23.0$ ), PCL film ( $50.0 \pm 7.0$  cells) and glass slide ( $10.0 \pm 3.0$  cells) (\*P < 0.05, \*\*P < 0.05, \*\*\*P < 0.05, • P < 0.05). Confocal micrographs of NG108-15 neuronal cells immunolabelled for beta-III tubulin grown on PHA blend/BG1 (Figures S3), and PHA blend/BG2 composites (Figure S4) shown in the supplementary material were taken with higher magnification in order to observe neurite bearing neurons. The growth and differentiation of NG108-15 cells on all the PHA blend composites confirmed that both BG types displayed high biocompatibility with neuronal cells.

The response of neuronal cells towards the substrates was further studied in co-culture with RN22 SCs in order to evaluate the effect of RN22 cells on neuronal differentiation and neurite outgrowth. Micrographs of NG108-15 neuronal cells (red) grown in co-culture with RN22 SCs (green) are shown in Figure 5 and Figures S3 of the supplementary material. Neuronal cells were immunolabelled for  $\beta$ -III tubulin (red) whereas RN22 cells were stained with S100 $\beta$  (green) for visualization. Neurite outgrowth assessment of NG108-15 neuronal cell/Schwann cell co-cultures was performed according to Daud [26].

As can be seen from Figure 5, only a few RN22 SCs were detected using the confocal microscope after four days of cell co-culture on the surface of the six PHA blend/BG composites. Detachment of RN22 SCs might have occurred during the process of cell fixation and washing required for the immunolabelling of the samples. Moreover, during cell growth previous to co-culture, detachment of RN22 SCs clots was observed concomitant to a faster growth compared to NG108-15 cells. Therefore, a quantitative analysis of RN22 SCs was not performed. While only small numbers of RN22 SCs were detected, analysis of NG108-15 neuronal cells demonstrated their ability to attach, grow and differentiate on all the substrates co-existing with RN22 SCs. As in the live/dead cell test and in the neurite outgrowth assessment of NG108-15 neuronal cells in single cultures, the PHA blend/BG1 (1.0 wt %) composite supported the highest number of differentiated neuronal cells when co-cultured with RN22 SCs ( $650.0 \pm 20.0$  cells) compared to the rest of substrates (Figure 5S). Statistical analysis of neuronal cells grown on the PHA blend/BG composites in single culture showed an increase in neuronal cell attachment when cultured with RN22 SCs except for the PHA blend/BG1 (0.5 wt %). This increase was statistically significant for all composites. A seven-fold increase was shown in the number of neuronal cells detected in the PHA blend/BG2 (1.0 wt %) and PHA blend/BG2 (2.5 wt%) when cultured with RN22 SCs.

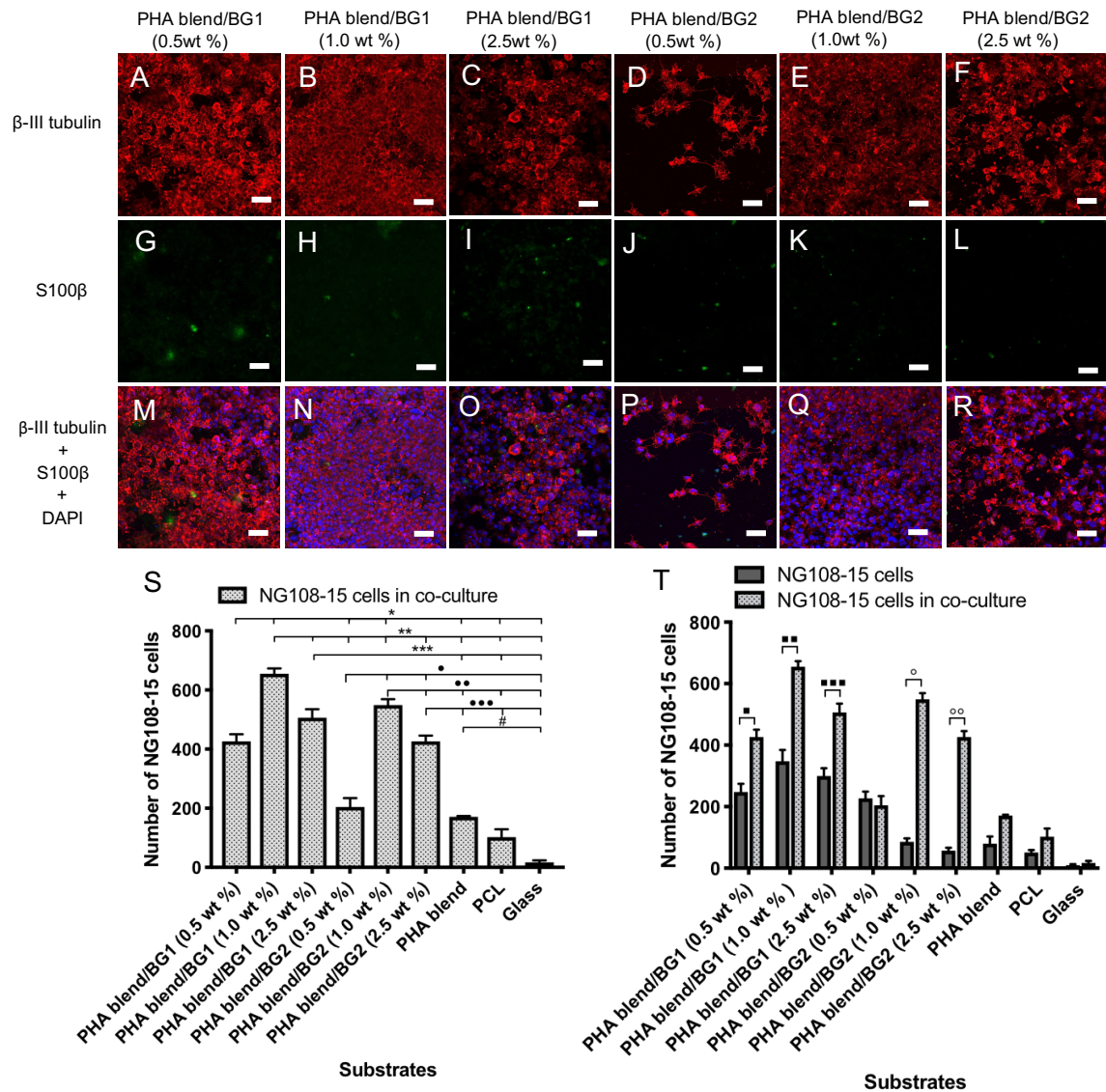


**Figure 5.** Micrographs of NG108-15 neuronal cells immunolabelled for  $\beta$ -III tubulin (red) grown in co-culture with RN22 SCs stained with S100 $\beta$  (green) after 4 days on PHA blend/bioactive glass composites. (A, G, M) PHA blend/BG1 (0.5 wt %); (B, H, N) PHA blend/BG1 (1.0 wt %); (C, I, O) PHA blend/BG1 (2.5 wt %); (D, J, P) PHA blend/BG2 (0.5 wt %); (E, K, Q) PHA blend/BG2 (1.0 wt %); (F, L, R) PHA blend/BG2 (2.5 wt %). S) Number of neuronal cells grown when co-cultured with RN22 SCs. T) Number of NG108-15 neuronal cells grown on the PHA blend/BG composites in single culture vs co-cultured with RN22 SCs.

The number of neuronal cells presented on PHA blend/BG1 (1.0 wt %) when grown with RN22 SCs was significantly different to that of PHA blend/BG1 (0.5 wt %) ( $*P < 0.05$ ) and to those of PHA blend/BG1 (2.5 wt %), PHA blend/BG2 (0.5 wt %), PHA blend/BG2 (1.0 wt %), PHA blend/BG2 (2.5 wt %), PHA blend film, PCL film ( $100.0 \pm 30.0$  cells) and glass ( $**P < 0.05$ ) (Figure

5). The number of neuronal cells grown on PHA blend/BG2 (1.0 wt %) in the presence of RN22 SCs was significantly different to that determined for the PHA blend/BG2 (2.5 wt %) ( $**P < 0.05$ ). A statistically significant increase was observed in the number of NG108-15 cells when grown in co-culture with RN22 SCs on the PHA blend/BG1 (0.5 wt %) ( $*P < 0.05$ ); PHA blend/BG1 (1.0 wt %) ( $**P < 0.05$ ); PHA blend/BG1 (2.5 wt %) ( $***P < 0.05$ ); PHA blend/BG2 (1.0 wt %) ( $^{\circ}P < 0.05$ ), and PHA blend/BG2 (2.5 wt %) ( $^{\circ\circ}P < 0.05$ ).

Bioactive glasses, such as BG1 and BG2 compositions are well known to react with phosphate ions present in the surrounding environment. These ions are commonly found in DMEM, which was used for culturing the cells in all the experiments described in this investigation. Once these bioactive glasses are submerged in a solution, they start to dissolve and release cations in the surrounding environment ( $Si^{2+}$ ,  $Ca^{2+}$ ,  $Na^{+}$ ,  $P^{+5}$  in both BGs; and  $K^{+}$  and  $Mg^{2+}$  in BG 1393). Hence, some of the phosphate ions present in the culture media may have reacted with some of the released calcium ions to form amorphous calcium phosphate and/or hydroxyapatite (HA). The resulting HA could have a beneficial effect on cell growth of differentiated neuronal cells by improving cell attachment. [27] In addition there are well-known effects of BGs upon contact with physiological fluids, including cell attachment and stimulation of growth factor production by their dissolved ions (i.e., vascular endothelial growth factor (VEGF); basic fibroblastic growth factor (bFGF)) [2]. Both, 45S5 and 1393 BGs release the cations  $Ca^{+2}$  and  $P^{+5}$  in physiological solutions, which have shown to stimulate angiogenesis. Phosphorous results in an increase in VEGF, bFGF, and matrix metalloproteinase-2 (MMP-2), whereas calcium has shown to enhance endothelial cell proliferation (Saghiri *et al.*, 2015). The combined effect of the above mentioned phenomena can explain the cellular growth increment observed in the composites, PHA blend/BG1 (0.5, 1.0, 2.5 % wt) and PHA blend/BG2 (0.5, 1.0 % wt) as compared to PHA-control films. Hence, the bonding between BG-containing surfaces and cells is the result of dissolution and precipitation reactions on the surface of the material. These interactions are highly affected by the BG composition and involve proteins absorbed to the material surface, cell



receptors and dissolved ions <sup>[2]</sup>. Therefore, while some of the phosphate and calcium ions could have reacted to form HA, other free phosphate and calcium ions could have been free in solution and entered the cell via the Na/Pico-transporter (NPT) (Prié *et al.*, 2001) and specific membrane channels respectively, positively affecting the expression of growth factors by neuronal cells. There are a great diversity of voltage- and ligand-gated ion channels that are permeable to inorganic ions such as calcium, sodium, potassium and chloride, which are vital for the electrical activity of excitable cells. Moreover, calcium in particular, as previously mentioned also serves as an essential signalling entity (Simms and Zamponi, 2016).

It is well-known that the hydrophobicity of surfaces significantly affect cell attachment. However, in this study a lack of linearity was observed in terms of hydrophobicity/cell growth. It is expected that lower water contact angles would support higher cell adhesion and growth. Although the composites with the lowest water contact angles, PHA blend/BG1 0.5 wt (65.7 ± 1.2 °) and PHA blend/BG1 1.0 wt % (65.3 ± 1.4 °) showed the best performance supporting cell growth of neuronal cells, the composite PHA blend/BG1 0.5 wt % with the highest contact angle, (95.7 ± 0.6 °) presented optimal biocompatibility (Fig. 4, 5, S3). The formation of a HA layer could potentially counteract the unfavourable effect of the hydrophobic surface in the PHA blend/BG1 0.5 wt % composite by providing a bonding interface. Similarly, the biocompatibility of the composite PHA blend/BG2 0.5 wt % (93.5 ± 0.8°) could also have been improved by the formation of a HA layer (Fig. 3, 4). Surprisingly an opposite effect was observed in the co-culture system of PHA blend/BG2 0.5 wt % in which addition of RN22 SCs could have a detrimental effect in cell growth by either hindering the formation of HA or by depleting the nutrients in the media. This composite was the only construct that showed a decrease in NG108-15 growth in co-culture with RN22 SCs.

Calcium ions also have a vital role in the initiation of the nerve regeneration process. When a nerve is damaged two signals are triggered for the promotion of regeneration; rapid calcium-based and slower retrograde transport-based signals. <sup>[28]</sup> Following axotomy, a localized transient elevation in the free intracellular calcium concentration provides a signal that triggers the formation of a growth

cone at the tip of the severed axon. [29,30] This transformation is a key step for a successful regeneration. Elevated calcium has also been found to support branching to postsynaptic targets and assist fusion of axonal targets.[30] Injury signals including transient elevation of calcium trigger activation of leucine kinase-1 DLK-1.[31] This kinase has shown to be required for growth cone formation in several organisms including *Caenorhabditis elegans* [30,32,33] *Drosophila* [34] and mice. [35] Since intracellular calcium concentration is fundamental for successful nerve regeneration, the use of bioactive glasses as calcium delivery systems with controlled released could improve axonal growth.

In all the cell culture experiments, PHA blend/BG1 (1.0 wt %) exhibited superior performance in supporting the growth of differentiated NG108-15 cells compared to the rest of substrates. The superior performance of PHA blend/BG1 (1.0 wt %) was consistent in all the cell culture experiments (live/dead analysis, neurite outgrowth assessment of NG108-15 neuronal cells and NG108-15/RN22 SCs co-cultures). Furthermore, neurite extension found in the PHA blend/BG1 (1.0 wt %) was very clear as observed in places where neurites formed a complex connection network (Supporting material, Figure S3). These interconnected neurite structures were also observed in PHA blend/BG1 (0.5 wt%) (Supporting material, Figure S3). The growth and differentiation of the NG108-15 cells on the remaining PHA blend/composites was variable in the live/dead cell test, neurite outgrowth assessment on NG108-15 neuronal cell and on NG108-15/RN22 SCs co-cultures. It is important to note that despite the fact that PHA blend/BG1 (1.0 wt%) displayed a superior performance as a neuronal scaffold, this composite did not show the most favourable surface characteristics among the rest of composites. Although the water contact angle ( $65.7 \pm 1.2^\circ$ ) corresponded to a hydrophilic substrate, the roughness was low and its microstructure did not show an interconnected porous system. Therefore, the concentration of BG1 used in PHA blend/BG1 might have played an important role in the favourable properties of this composite, by providing a beneficial balance of cations in the culture media. It is worth to mention that this is the first study of PHA/BG composites in the context of neural tissue engineering.

In general, both BGs showed significant biocompatibility within the PHA blend. In all the experiments the presence of BGs at all concentrations (0.5 wt %, 1.0 wt %, 2.5 wt %) increased the number of neuronal cells with respect to both, the PHA blend control and PCL control. The 45S5 composites exhibited better performance in supporting cell growth and differentiation of NG108-15 cells, compared with the BG2 composites.

To the best of our knowledge, this study is the first to evaluate the effect of BG2 on neuronal regeneration and shows its potential application as a base material in the form of PHA/BG2 composite for the manufacture of inner structures of NGCs used for regeneration of peripheral nerves. In contrast, BG1 has been previously investigated for peripheral nerve regeneration applications, either on its own or in combination with other polymers, but not PHAs. Bunting <sup>[3]</sup> have reported that fibres of BG1 are biocompatible with rat SCs and fibroblasts *in vitro*. They showed qualitative and quantitative evidence of axonal regeneration *in vivo* using a silastic conduit filled with BG1 fibres implanted in sciatic nerves of adult rats. Additionally, Mohammadkhah <sup>[7]</sup> used BG1 as one of the components of a range of poly- $\epsilon$ -caprolactone (PCL)/BG composites used to support nerve regeneration. For the biocompatibility study, dorsal root ganglia (DRG) isolated from embryonic chicks was cultured on composite sheets and neurite outgrowth was measured. The bioactive glass particles added to the composites did not show any negative effects on neurite extension. An increase in neurite outgrowth of DRG cultured on the poly- $\epsilon$ -caprolactone (PCL) / BG1 composite was observed compared with PCL sheets. <sup>[7]</sup>

Although only few RN22 SCs were detectable at the end of the experiment, they may have supported neuronal growth and axon extension. RN22 SCs grow faster than NG108-15 cells and form a layer of cells that tend to detach easily. Therefore, RN22 SCs could have detached during the fixation and washing process prior to immunolabelling. SCs are the myelin-forming cells of the peripheral nervous system. SC-neuron communication is carried out through intracellular waves of calcium and via intercellular diffusion of chemical messengers, which are involved in the synaptic

transmission.<sup>[36,37]</sup> In this respect, the release of  $\text{Ca}^{2+}$  from bioactive glasses could be controlled to obtain a beneficial effect in SC-neuron communication.

Intercalated regions of myelinated sheets leave the axonal section of the neuronal cells exposed to promote the depolarization of the membrane. Nodes of Ranvier are rich in voltage-gated  $\text{Na}^+$  channels, where  $\text{Na}^+$  ions cross and depolarize the membrane between segments of compacted myelin. Herein, the release of  $\text{Na}^+$  ions from bioactive glasses might have an effect on the membrane polarization during impulse conduction. Further research needs to be carried out to investigate the specific effect of the  $\text{Na}^+$  ions released from bioactive glasses on the membrane polarization.

#### **4. Conclusions**

The microstructure of the PHA blend/BG composites were affected by the concentration of bioactive glasses in the composite. The concentration of BG1 and BG2 showed an effect not only in the pore size of PHA blend/BG composites, but also in the distribution and structure of the porous systems. The efficient growth and differentiation of NG108-15 cells on all the PHA blend composites confirmed that both bioactive glasses (BG1 and BG2) have good biocompatibility when used as a PHA blend composite. The growth and differentiation of NG108-15 cells on PHA blend/composites was found to be variable in the live/dead cell test and neurite outgrowth assessment. In general, both bioactive glasses exhibited a significant impact on the biocompatibility of the PHA blend. Although composites with BG2 were shown to support neuronal regeneration, composites with BG1 displayed superior performance in supporting cell growth and differentiation of neuronal cells. The presence of RN22 SCs in NG108-15 cultures had a further positive effect on the growth and maintenance of the differentiated neuronal cells on all the PHA blend/composites except for the PHA blend/BG2 (0.5 wt %). PHA blend/BG1 (1.0 wt %) exhibited the best performance in supporting growth and maintaining neuronal differentiation of NG108-15 amongst all the substrates in all the cell culture experiments. Moreover, neurite extension found on the PHA blend/BG1 (1.0 wt%) was remarkable, as neurites formed a complex connection network. Therefore, the PHA blend/BG1 (1.0 wt%)

exhibited the best combination of surface features, chemical and mechanical properties to emerge as the best substrate for the growth and differentiation of neuronal cells and hence for the future development of both lumen structures of NGCs and for nerve tissue regeneration in general.

### **Author information**

#### **Corresponding author:**

#### **E-mail:**

i.roy@sheffield.ac.uk

#### **ORCID**

**Ipsita Roy:** <https://orcid.org/0000-0001-5602-1714>

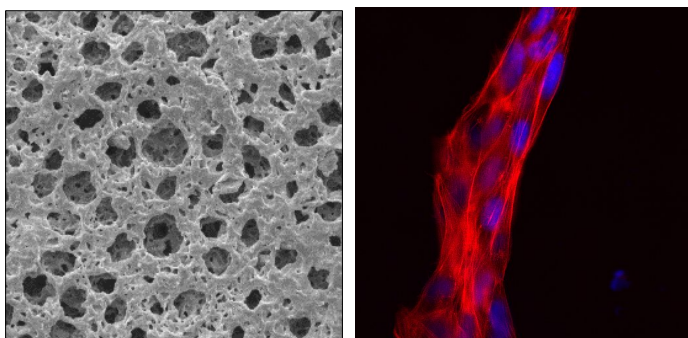
### **Acknowledgements**

The authors would like to acknowledge the Department of Materials Science and Engineering (Kroto Research Institute, University of Sheffield, UK), NEURIMP, Grant Agreement No. 604450, a Framework 7 project funded by the EC, and University of Westminster for providing the facilities, materials, and funding for this research work. The authors would also acknowledge Rosa Angelica L. Valderrama and Raul Lizarraga for providing funding for this investigation.

### **Conflict of Interest**

The authors declare no conflict of interest.

### **Grafical abtract**



- 1.- Novajra, G.; Tonda-Turo, C.; Vitale-Brovarone, C.; Ciardelli, G.; Geuna, S.; Raimondo, S. Novel systems for tailored neurotrophic factor release based on hydrogel and resorbable glass hollow fibers. *Materials Science and Engineering C*. 2014, *36*, 25–32.
- 2.- Miguez-Pacheco, V.; Hench, L. L., Boccaccini, A. R. Bioactive glasses beyond bone and teeth: emerging applications in contact with soft tissue. *Acta Biomaterialia*. 2015, *13*, 1-15.
- 3.- Bunting, S.; Di Silvo, L.; Deb, S.; Hall, S. Bioresorbable Glass Fibres Facilitate Peripheral Nerve Regeneration. *Journal of Hand Surgery*. 2005, *30*, 242-247.
- 4.- Vitale-Brovarone, C.; Novajra, G.; Lousteau, J.; Milanese, D.; Raimondo, S.; Fornaro, M. Phosphate glass fibres and their role in neuronal polarization and axonal growth direction. *Acta Biomaterialia*. 2012, *8*, 1125–1136.
- 5.- Kim, D-S.; Li, K-W.; Boroujerdi, A.; Yu, Y.P.; Zhou, C-Y.; Deng, P.; Park, J.; Zhang, X.; Lee, J.; Corpe, M.; Sharp, K.; Steward, O.; Eroglu, C.; Barres, B.; Zaucke, F.; Xu, Z.C.; Luo, Z.D. Thrombospondin-4 contributes to spinal sensitization and neuropathic pain states. *The Journal of Neuroscience*. 2012, *32*, 8977-8987
- 6.- Marquardt, L. M.; Day, D.; Sakiyama-Elbert, S. E; Harkins, A. B. Effects of borate-based bioactive glass on neuron viability and neurite extension. *Journal of Biomedical Material Research - Part A*. 2014, *102*, 2767–2775.
- 7.- Mohammadkhah, A.; Marquardt, L.M.; Sakiyama-Elbert, S. E.; Day, D. E.; Harkins, A. B. Fabrication and characterization of poly-( $\epsilon$ )-caprolactone and bioactive glass composites for tissue engineering applications. *Materials Science and Engineering. C, Materials for Biological Applications*. 2015, *49*, 632–639.
- 8.- Alhashimi, R. A.; Mannocci, F.; Sauro, S. Bioactivity, cytocompatibility and thermal properties of experimental Bioglass-reinforced composites as potential root-canal filling materials. *Journal of the Mechanical Behavior of Biomedical Materials*. 2017, *69*, 355–61.

- 9.- Cui, N., Qian, J., Wang, J.; Ji, C.; Xu, W.; Wang, H. Preparation, physicochemical properties and biocompatibility of PBLG/PLGA/bioglass composite scaffolds. *Materials Science and Engineering: C*. 2017, *71*, 118–24.
- 10.- Lizarraga-Valderrama, L.R.; Nigmatullin, R.; Taylor, C., Haycock, J.W.; Claeysens, F.; Knowles, J.C.; I. Roy. Nerve tissue engineering using blends of poly(3-hydroxyalkanoates) for peripheral nerve regeneration. *Engineering in Life Sciences*. 2015, *15*, 612–621.
- 11.- Rai, R.; Yunos, D. M.; Boccaccini, A. R.; Knowles, J. C.; Barker, I. A.; Howdle, S. M.; Tredwell, G. D.; Keshavarz, T. S.; Roy, I. Poly-3-hydroxyoctanoate P(3HO), a medium chain length polyhydroxyalkanoate homopolymer from *Pseudomonas mendocina*. *Biomacromolecules*. 2011, *12*, 2126-2136.
- 12.- Desmond, K. W.; Weeks, E. R. Influence of particle size distribution on random close packing of spheres. *Physical Review E*. 2014, *90*, 1-6.
- 13.- Alam, P. Porous Particle-Polymer Composites. *Advances in Composite Materials - Analysis of Natural and Man-Made Materials*. 2011, *2*, 29-54.
- 14.- Chiono, V.; Tonda-Turo, C. Trends in the design of nerve guidance channels in peripheral nerve tissue engineering. *Progress in Neurobiology*. 2015, *131*, 87–104.
- 15.- Goddard, J. M.; Hotchkiss, J. H. Polymer surface modification for the attachment of bioactive compounds. *Progress in Polymer Science (Oxford)*. 2007, *32*, 698–725.
- 16.- Xu, Z.; Choudhary, S.; Okada, Y.; Voznesensky, O.; Alander, C.; Raisz, L.; Pilbeam C. Cyclooxygenase-2 gene disruption promotes proliferation of murine calvarial osteoblasts in vitro. *Bone*. 2007, *41*, 68–76.
- 17.- Tamada, Y., Ikada, Y. Effect of preadsorbed proteins on cell adhesion to polymer surfaces *Journal of Colloid and Interface Science*. 1993, *155*, 334–339.

- 18.- Wei, J.; Igarashi, T.; Okumori, N.; Igarashi, T.; Maetani, T.; Liu, B.; Yoshinari M. Influence of surface wettability on competitive protein adsorption and initial attachment of osteoblasts. *Biomedical Materials*. 2009, 4, 1-7.
- 19.- Vogler, E. A. Water and the acute biological response to surfaces. *Journal of Biomaterials Science, Polymer Edition*. 1999, 10, 1015–1045. <https://doi.org/10.1163/156856299X00667>
- 20.- Yildirim, E. D.; Besunder, R.; Pappas, D.; Allen, F.; Güçeri, S.; Sun, W. Accelerated differentiation of osteoblast cells on polycaprolactone scaffolds driven by a combined effect of protein coating and plasma modification. *Biofabrication*. 2010, 2, 1-12
- 21.- Khorasani, M.T.; Mirzadeh, H.; Irani, S. Plasma surface modification of poly (l-lactic acid) and poly (lactic-co-glycolic acid) films for improvement of nerve cells adhesion. *Radiation Physics and Chemistry*. 2008, 77, 280–287.
- 22.- Lee, A. C.; Yu, V. M.; Lowe, J. B.; Brenner, M. J.; Hunter, D.A.; Mackinnon, S.E.; Sakiyama-Elbert, S.E. Controlled release of nerve growth factor enhances sciatic nerve regeneration. *Experimental Neurology*. 2003, 184, 295–303.
- 23.- Barham, P.J.; Keller, A.; Otun E. L.; Holmes, P.A. Crystallization and morphology of a bacterial thermoplastic: poly-3-hydroxybutyrate. *Journal of Materials Science*. 1984, 19, 2781–2794.
- 24.- Schick, C.; Wurm, A.; Mohamed, A. Vitrification and devitrification of the rigid amorphous fraction of semicrystalline polymers revealed from frequency-dependent heat capacity. *Colloid and Polymer Science*. 2001, 279, 800–806.
- 25.- Al-Nasassrah, M. A.; Podczek, F.; Newton, J. M. The effect of an increase in chain length on the mechanical properties of polyethylene glycols. *European Journal of Pharmaceutics and Biopharmaceutics*. 1998, 46, 31–38.



- 26.- Daud, M. F. B.; Pawar, K. C, Claeysens, F.; Ryan, A. J., Haycock, J. W. An aligned 3D neuronal-glia co-culture model for peripheral nerve studies. *Biomaterials*. 2012, 33, 5901–5913.
- 27.- Huang, W.; Day, D. E.; Kittiratanapiboon, K.; Rahaman, M. N. Kinetics and mechanisms of the conversion of silicate (45S5), borate, and borosilicate glasses to hydroxyapatite in dilute phosphate solutions. *Journal of Materials Science: Materials in Medicine*. 2006, 17, 583–596.
- 28.- Ferguson, T. A.; Son, Y. J. Extrinsic and intrinsic determinants of nerve regeneration. *Journal of Tissue Engineering*. 2011, 2, 1–12.
- 29.- Ziv, N. E.; Spira, M. E. Localized and transient elevations of intracellular Ca<sup>2+</sup> induce the dedifferentiation of axonal segments into growth cones. *The Journal of Neuroscience : The Official Journal of the Society for Neuroscience*. 1997, 17, 3568–3579.
- 30.- Ghosh-Roy, A.; Wu, Z.; Goncharov, A.; Jin, Y.; Chisholm, A. D. Calcium and Cyclic AMP Promote Axonal Regeneration in *Caenorhabditis elegans* and Require DLK-1 Kinase. *Journal of Neuroscience*. 2010, 30, 3175–3183.
- 31.- Tedeschi, A.; Bradke, F. The DLK signalling pathway—a double-edged sword in neural development and regeneration. *EMBO Reports*. 2013, 14, 605–614.
- 32.- Hammarlund, M.; Nix, P.; Hauth, L.; Jorgensen, E. M.; Bastiani, M. Axon regeneration requires a conserved MAP kinase pathway. *Science*. 2009, 323, 802-806.
- 33.- Byrne, A. B., Hammarlund, M. Axon regeneration in *C. elegans*: Worming our way to mechanisms of axon regeneration. *Experimental Neurology*. 2017, 287, 300–309.
- 34.- Xiong, X.; Wang, X.; Ewanek, R.; Bhat, P.; DiAntonio, A.; Collins, C. A. Protein turnover of the Wallenda/DLK kinase regulates a retrograde response to axonal injury. *Journal of Cell Biology*, 2010, 19, 211–223.
- 35.- Itoh, A.; Horiuchi, M.; Bannerman, P.; Pleasure, D.; Itoh, T. Impaired regenerative response of primary sensory neurons in ZPK/DLK gene-trap mice. *Biochemical and Biophysical Research Communications*. 2009, 383, 258–262.

36.- Sugiura, Y.; Lin, W. Neuron-glia interactions: the roles of SCs in neuromuscular synapse formation and function. *Bioscience Reports*. 2011, *31*, 295–302.

37.- Zargar Kharazi A.; Dini, G.; Naser, R. Fabrication and evaluation of a nerve guidance conduit capable of Ca<sup>2+</sup> ion release to accelerate axon extension in peripheral nerve regeneration. *Journal of Biomedical Materials Research Part A*. 2018, *106A*, 2181–2189.